DISCLAIMER

UNDERSTANDING THE EFFECTS OF COMPRESSION AND CONSTRAINTS ON WATER UPTAKE OF FUEL-CELL MEMBRANES

Ahmet Kusoglu[*], Brian L. Kienitz [†,*], Adam Z. Weber [‡,*]
Environmental Energy Technologies Division, Lawrence Berkeley National Laboratory, One Cyclotron Road, Berkeley CA 94720, USA

Accurate characterization of polymer-electrolyte fuel cells (PEFCs) requires understanding the impact of mechanical and electrochemical loads on cell components. An essential aspect of this relationship is the effect of compression on the polymer membrane's water-uptake behavior and transport properties. However, there is limited information on the impact of physical constraints on membrane properties. In this paper, we investigate both theoretically and experimentally how the water uptake of Nafion membrane changes under external compression loads. The swelling of a compressed membrane is modeled by modifying the swelling pressure in the polymer backbone which relies on the changes in the microscopic volume of the polymer. The model successfully predicts the water content of the compressed membrane measured through in-situ swelling-compression tests and neutron imaging. The results show that external mechanical loads could reduce the water content and conductivity of the membrane, especially at lower temperatures, higher humidities, and in liquid water. The modeling framework and experimental data provide valuable insight for the swelling and conductivity of constrained and compressed membranes, which are of interest in electrochemical devices such as batteries and fuel cells.

† Current Address: W.L. Gore and Associates, 201 Airport Road, Elkton, MD USA
‡ Corresponding author. E-mail address: azweber@lbl.gov Tel: (510) 486-6308.
* ECS Member.

Keywords: PFSA, Nafion® membrane, fuel cells, swelling pressure, compression, neutron imaging, mathematical model.

Introduction

Ionomer membranes used in polymer-electrolyte-fuel-cell (PEFC) applications are always subjected to mechanical constraints to some extent due to cell design and clamping loads to reduce contact resistances and seal cells using compression seals. Furthermore, swelling of the membranes due to water uptake results in compressive stresses during cell operation.[1-3] Compression in the cell is known to influence membrane stresses,[2-6] transport in gas-diffusion layers (GDL),[7-9] and cell resistance.[10] However, the effect of the constraints and mechanical loads on the membrane's water-uptake behavior is yet to be determined due to the difficulty of such measurement. Moreover, due to the lack of the experimental data on the swelling behavior of constrained membranes, mathematical models on water uptake cannot be fully validated. In this work, we aim to investigate how the constraints on the membrane affect its water-uptake behavior and other water-dependent transport properties such as conductivity.

In a PEFC, the extent to which the membrane is deformed depends on a number of factors including, but not limited to, geometry of the cell (e.g. land/channel ratio), thickness and stiffness of the cell components (e.g. bipolar plates, gas-diffusion layers (GDLs)), and operating conditions (e.g., humidity). Thus, stresses and pressures in the membrane are not uniform; they depend on location, time, and component material properties. In addition, the membrane itself is subjected to a combination of constraints and mechanical loads: (i) interfacial constraints arising between the membrane and electrodes during the MEA manufacturing, (ii) pressure on membrane (or MEA) surface during cell assembly due to the clamping force coming from the endplates through the diffusion media. (iii) loads arising during cell operation such as the compressive stresses induced by the swelling of the somewhat constrained membrane during

hydration (both in the plane and in the thickness direction).[2,4-6] We note that the pressure in the second case is external to the membrane and explicitly controlled independent of the membrane's water content, whereas in the last case it is determined implicitly by the membrane's water-uptake behavior, which in turn could be limited by the pressure.

In addition, there could be other internal constraints developed in the membrane during the manufacturing process. For example, extruded or stretched membranes exhibit structural anisotropy due to the preferential orientation during extrusion process that gives the membrane improved mechanical properties and lower swelling in the extrusion direction.[11-13] Moreover, membranes that are macroscopically reinforced with ePTFE have almost negligible swelling in the plane (reinforcement) direction and much higher mechanical properties.[14,15] However, these constraints are internal and therefore all the resulting effects become an inherent property of the membrane. For example, reinforcing the membrane with a stiffer material would generate additional internal resistance to the swelling in the direction of the reinforcement. This effect is similar to, at least theoretically, externally constraining an unreinforced membrane in one direction and letting it hydrate; it will swell less in the constrained direction compared to the unconstrained direction. Thus, we see the effect of internal constraints on water uptake, conductivity, swelling, etc. to a certain degree in most commercial polymer fuel-cell membranes. However, how these constraints and especially compressive loads control and alter a membrane's properties through morphological changes is yet to be determined.

A number of recent publications on the in-situ neutron imaging of water in PEFCs have provided evidence on the change in the membrane water content upon increasing the cell compression.[16,17] The compression effect has been studied at the cell- and component- scale, yet

the concept of pressure changes when it comes to the pressure within the swollen domains of the membrane at the nanometer lengthscale.[18-20] There are a limited number of studies focused on measuring the swelling pressure in the membrane using custom-made fixtures and reported pressures between 30-100 MPa.[21-23] Moreover, except for a few studies investigating the constraints in PEFCs,[1,3,24] mathematical models generally assume that membranes are unconstrained (although with a given thickness, i.e., swelling is ignored). In fact, there has been only minimal research into swelling of constrained polymers in general with notable exceptions of gels and elastomers, for which Flory-Rehner theory[25,26] is commonly employed to develop models.[27-29] However, it is debatable that these models, at least in their current form, are applicable to semi-crystalline perfluorinated membranes due to these membranes' much different mechanical and uptake properties and relationships, which stem from their different intrinsic morphology in comparison to gels and elastomers that contain significant amounts of water and deform much easier and without internal crystallite structures. Therefore, the water uptake of compressed/constrained ionomers warrants further investigation, both theoretically and experimentally.

For PEFCs, Weber and Newman[1] studied the effect of constraints on the water-uptake behavior and conductivity of membranes by means of a macro-homogenous membrane model. Kusoglu et al.[19] developed a mechanics-based model for the swelling pressure in ionomers by accounting for the microscale swelling. In this work, we build on the concepts of both of those efforts and develop a mathematical model for the water uptake of ionomer membranes that accounts for compression effects and validate it with experimental data. In the following, first we describe the experiments undergone to measure swelling pressures and water uptake under

compressions. Next, the mathematical modeling methodology is discussed with a focus on water uptake using chemical-potential equilibrium for cases with and without compression or constraint. Then the validation of the model is presented with both our own and literature experimental data. Finally, the impact of compression and constraint on transport properties is discussed.

Experimental

Swelling Measurements under Compression

Nafion® 117 membranes (1100 g/molSO_3) were obtained from Ion Power Inc. (New Castle, DE). Membranes were boiled for an hour each, in succession, in deionized (DI) water, 3% hydrogen peroxide, DI water, and 0.5 M sulfuric acid in accordance with standard pretreatment method in the literature.[30] Compression tests for the membranes were carried out using an Instron electromechanical testing machine equipped with linear-variable-displacement transducers (LVDTs) with 0.5 micron resolution (Solartron Metrology) for thickness measurement. Tests were conducted at ambient temperature. A cylindrical stainless steel compression fixture (Figure 2) designed by Budinski and Cook[21] was used for the in-situ compression tests. The fixture consists of a hollow cylinder of 10 mm inner diameter, a hydrophilic frit on which the sample sits, and a water reservoir in the bottom. The fixture was placed between the compression platens of the testing machine where the piston transfers the load from the machine directly to the sample. After the sample was placed in the fixture, it was allowed to swell and equilibrate with the DI water from the reservoir that contacts the sample

through the frit. During liquid-equilibrium, the sample-thickness change (swelling) was continuously recorded via the LVDTs. Then, by applying pressure to the hydrated sample via the piston, change in the thickness (de-swelling) of the sample is measured as a function of compression load (pressure). The membrane is always in contact with water through the hydrophilic frit enabling in-situ hydrostatic-compression tests. The area of the sample is constant and therefore the change in thickness can be used to determine directly the change in water content.

Neutron Imaging

To investigate the effect of compression on the swelling of the membrane alone, we used a simple test setup to measure the water content via neutron imaging. The setup involves compressing the membrane between aluminum plates under a controlled load, and then determining the change in water content from 2D neutron radiographs of compressed and uncompressed liquid-equilibrated membranes. The tests were performed at McClellan Nuclear Radiation Center (MNRC) in Davis, CA. Scintillation screen resolution of the setup was 100 μm. To obtain more accurate information on the thickness reduction, 750 micron (30 mil) thick custom-made PFSA membranes in H^+ form with 1100 and 1000 g/mol equivalent weight (EW) (Ion Power, New Castle, DE) were used for the experiments. Dry samples were prepared by drying the membranes for an hour using vacuum-assisted heating at 80 °C. Then, samples were liquid-equilibrated and kept in DI water for at least a day prior to imaging. The dimensions and weight of the samples were recorded for each sample before imaging with typically square areas of 4 in^2. First, images were taken for the dry and wet samples by placing them between

aluminum plates (without compression) that were much larger than the membrane area. Then, another image for the wet sample was taken after the plates were compressed by applying a constant torque to the bolts using a digital torque wrench; two compression levels were used corresponding to the pressures of 2 and 4 MPa. Neutron radiographs of the samples in the fixture were taken for both face-on (surface) and edge-on (thickness) directions.

Theoretical

Equilibrium water uptake

Before discussing constraint and compression, a model should be developed for the free-swelling (unconstrained) case. The swelling process of the membrane can be described microscopically as the solvation of ionic groups by the external water vapor and then the formation of hydrophilic water-filled domains, so-called clusters, at nanometer lengthscales. Initial water molecules ionize the SO_3^- groups and remain bound to them. Additional water molecules are free to move through the ionomer nanostructure, causing growth of the water domains and consequently the macroscopic swelling of the membrane. These water domains are separated from the hydrophobic polymer matrix forming various shapes resulting in a two-phase nanostructure.[31-42] As the water-uptake increases, these water domains grow, and in some cases coalesce or change shape,[11,32,33,35,38,43-46] causing continuous structural reorganization in the swollen polymer. Consequently, microscopic strain of the inter-domain spacing is higher than the macroscopic swelling strain.[11,31-33,35,38,39,42,44,47] However, the growth of the water domains deforms the hydrophobic backbone surrounding these domains which decreases the osmotic pressure and therefore limits the swelling.[20,44,48-52] Consequently, swelling of a membrane at a

given humidity and temperature is governed by the equilibrium of the chemical-potential of water (having the same reference state)

$$\mu_{\mathrm{w}}^{e} = RT \ln a_{\mathrm{w}} = \mu_{\mathrm{w}}^{p} = RT \ln a_{\mathrm{p}} + \overline{V}_{\mathrm{w}} \Pi(p_{\mathrm{s}}) \quad [1]$$

where μ_{w}^{e} and μ_{w}^{p} are the chemical potential for water external and internal to the membrane, respectively, a_{w} and a_{p} are the activity of the water external and internal to the membrane, respectively, T is the absolute temperature, R is the universal gas constant, $\overline{V}_{\mathrm{w}}$ is the molar volume of water, and Π is the osmotic pressure. For equilibrium swelling, the osmotic pressure must equal the swelling pressure, p_{s}, applied by the polymer matrix to the water domains. The water activity internal to the membrane can be expressed using the Flory-Huggins (FH) theory for polymer solutions,[25]

$$\ln a_{\mathrm{p}} = \ln\left(1-\phi'_{\mathrm{p}}\right) + \left[\left(1-\frac{1}{\overline{V}_{\mathrm{p}}/\overline{V}_{\mathrm{w}}}\right)\phi'_{\mathrm{p}} + \chi\phi'^{2}_{\mathrm{p}}\right] \quad [2]$$

where χ is Flory–Huggins interaction parameter, which characterizes the enthalpic interactions of mixing between the polymer and solvent, and ϕ'_{p} is the volume fraction of the polymer including the bound water, i.e.

$$\phi'_{\mathrm{p}} = \frac{\overline{V}_{\mathrm{p}} + \lambda^{B}\overline{V}_{\mathrm{w}}}{\overline{V}_{\mathrm{p}} + \lambda\overline{V}_{\mathrm{w}}} \quad [3]$$

where λ is the total water content (mol H_2O per mol SO_3^-) and λ^{B} is the bound water that is strongly attached to ionic groups and is calculated in references [48,53,54]. Thus, the total water

content in the membrane consists of chemically bound water and free water.[20,37,48,54-57] The molar volume of the dry polymer,

$$\bar{V}_{\mathrm{p}} = EW / \rho_{\mathrm{p}}, \qquad [4]$$

is related to the equivalent weight (*EW*) of the membrane and its dry density, ρ_{p}.

As the interaction parameter of a solvent/polymer network decreases, solvent uptake becomes more favorable. The interaction parameter could be determined empirically, for example by fitting the FH expression to experimental water-uptake data. For PFSA membranes, the reported values for χ are between 0.9 and 2.5 with a strong dependence on the water content.[48,58,59] To account for both temperature and swelling effects, the following expression for the interaction parameter was found to be the best at predicting the sorption isotherms of Nafion membrane (Figure 3a):

$$\chi(\phi_{\mathrm{p}}, T) = \chi_S \phi_{\mathrm{p}}^{1.5} + \chi_T \left(1 - \frac{T}{T_{\mathrm{ref}}}\right) \qquad [5]$$

where χ_S and χ_T are the components of the interaction parameter controlling the swelling and temperature effects, respectively, and T_{ref} = 298K is the reference temperature. Eq. [5] suggests that swelling becomes more favorable with decreasing polymer volume fraction or increasing water content (e.g., $\chi \propto 1/\lambda$). However, an opposite effect is observed for temperature, i.e. the water content of vapor-equilibrated membranes decreases with increasing temperature.[54,58,60-62] This reduced uptake with temperature has been attributed to the changing hydrophilicity due to the surface interactions,[30,61,63] drying of water pores in the membrane,[64] and, more recently, to the changes in entropy of water and polymer-solvent interactions.[65,66] While the underlying

phenomena for reduced uptake at elevated temperatures are still not definitively known for Nafion membranes, it has been observed and is well-known in crosslinked and networked systems.[67] Thus, if one envisions the hydrophobic regions as physical crosslinks that change with membrane hydration due to the swollen hydrophilic domains, then one would predict lower water contents for vapor-equilibrated membranes at higher temperatures. For the analysis presented herein, the temperature effect on uptake of a vapor-equilibrated membrane is implemented into Eq. [5] simply using a non-zero χ_T to account for the observed phenomenon. However, as the reduced uptake at high temperatures does not occur for liquid-equilibrated membranes,[30,56,68,69] for which the water content is around $\lambda = 21$ to 23 H_2O/SO_3, χ_T can be set to zero in liquid water. Thus, the parameter χ_T can be attributed to the polymer-solvent interactions arising from the change in the phase of water and the associated changes in membrane morphology. We note that χ_T could also be related to the thermal history and pretreatment of the membrane, which are known to affect the water-uptake behavior of the membrane.[30,63,68,70,71]

Therefore, using the above expressions in Eq. [1], an implicit equation can be written to determine the water uptake of a PFSA membrane,

$$\left(1-\phi_{\mathrm{p}}'\right)\exp\left[\left(1-\frac{1}{\bar{V}_{\mathrm{p}}/\bar{V}_{\mathrm{w}}}\right)\phi_{\mathrm{p}}'+\chi(\phi_{\mathrm{p}},T)\phi_{\mathrm{p}}'^{2}\right]-a_{\mathrm{w}}\exp\left(-\frac{\bar{V}_{\mathrm{w}}}{RT}\Pi\left(\phi_{\mathrm{p}},T\right)\right)=0\,. \qquad [6]$$

Swelling pressure

To solve Eq. [6], one needs to know the swelling pressure function, $\Pi(\phi_p, T)$. Several approaches exist in literature to correlate the swelling pressure to the water volume fraction.[18-20,62] In this work, we adopt and modify the geometry-dependent pressure model in reference [19]. Swelling pressure can be interpreted as the pressure generated in the polymer matrix in response to growing water domains to balance the osmotic pressure. It is difficult to quantify the swelling pressure due to the complex nature of the swelling process in a polymer/water structure that evolves at multiple lengthscales. Therefore, it is helpful to find out how swelling pressure can be correlated with other measurable quantities that characterize the swelling. For example, the membrane's dimensional change is a useful quantity to determine the water content and swelling. However, understanding the underlying driving forces for sorption requires information on dimensional changes at multiple lengthscales. One such important description is the microscopic swelling, i.e., change in the distance between water domains, d-*spacing*, during water uptake (Figure 3b). The findings of SAXS experiments conducted at different humidities[31-33,35,38,39,42,44,47] suggest that the plot of macroscopic swelling vs. *d*-spacing is linear;

$$\frac{d}{d_{\text{dry}}} - 1 = k_s \left(\frac{L}{L_{\text{dry}}} - 1 \right) = k_s \left(\left(\frac{V}{V_{\text{dry}}} \right)^{-1/3} - 1 \right), \qquad [7]$$

where k_s is the swelling ratio that correlates the deformation at macroscales (i.e., sample length ~L) and nanoscales (i.e., domain spacing ~d). Interestingly, as seen in Figure 3b, the value of k_s is 5.0 to 5.6, i.e., higher than unity. This phenomenon could be attributed to the coalescence of the water domains and/or morphological transitions.[11,32,33,38,42,44] Essentially, the internal

structure of the hydrophilic domains change with water uptake due to the changing equilibrium between the mechanical compression of the backbones and the energy of hydration and interaction of the side chains. These interactions result in a change in the domain shape and morphology (e.g., spheres to cylinders), which are not easily interpreted from the SAXS data, although do result in a different domain spacing (i.e., domain spacing is a relatively gross measure of domain morphology). Thus, the higher than unity slope can be explained by such morphological rearrangements; although definitive results (e.g., electron micrographs) for Nafion membranes are still an open topic of research.

Since the swelling pressure is related to the deformation of the polymer matrix around the water domains, it is appropriate to use *d*-spacing to characterize swelling pressure. Swelling pressure then can be determined using a mechanics approach[19] for the simplified nanostructural descriptions of swollen PFSA membranes, e.g. spherical[38,50,72] or cylindrical[40] water domains. For the model, the nanostructure is represented by equal-sized microscopic volume elements (Figure 1), with an inner domain of pore (ion + water) surrounded by a concentric, outer domain of polymer matrix.[19] Assuming swelling is a quasi-static process, microscopic deformation of the polymer matrix is modeled by using linear elastic springs of length Δ compressed between the growing hydrophilic domains throughout the membrane (Figure 1). The springs are assumed to have the temperature-dependent modulus of the polymer backbone, $E_{\mathrm{pm}} = E_{\mathrm{pm}}(T)$.[19] Thus, the normalized pressure generated in the network, p_s / E_{pm}, is due to the radial deformation of the backbone during swelling from the dry state,

$$\frac{\Pi(\phi_w, T)}{E_{pm}(T)} = \frac{p_s}{E_{pm}} = 1 - \frac{\Delta}{\Delta_{dry}} = 1 - \frac{\frac{1}{2}d - r}{\frac{1}{2}d_{dry} - r_{dry}} = 1 - \frac{d}{d_{dry}}\left(\frac{1-\phi_{pore}^{1/n}}{1-\phi_{pore}^{dry\,1/n}}\right) \quad [8]$$

where r is the radius of the hydrophilic water domains (Figure 1), n is the dimension of the morphology (e.g. $n = 2$ for cylindrical domains and 3 for spherical domains) and $\phi_{pore} = (2r/d)^n$ from geometry. The temperature dependence is implemented into Young's modulus of the polymer backbone using the relationship $E_{pm} = 3.1(400 - T)$ which was calculated from the measured data in reference 19. When the membrane is completely dry, it is assumed that the domains contain only the SO_3^- groups. Therefore, ϕ_{pore}^{dry} must be equal to the SO_3^- volume fraction of a dry PFSA membrane,

$$\phi_{pore}^{dry} = \phi_{SO_3}^{dry} = \frac{\bar{V}_{SO_3}}{\bar{V}_p} = \frac{\bar{V}_{SO_3}}{EW/\rho_p} \quad [9]$$

where $\bar{V}_{SO_3}$ can be taken to be 40.94 cm^3/mol,[38] and the pore volume fraction becomes

$$\phi_{pore} = \phi_w + (1 - \phi_w)\phi_{pore}^{dry} \quad [10]$$

Using the expressions for the interaction parameter (Eq. [5]) and swelling pressure (Eq. [8]) in the equilibrium equation (Eq. [6]), water content is determined as a function of vapor-phase water activity. Our investigations show that the proposed expression for the interaction parameter, Eq. [5] with $\chi_s = 1.9$, successfully reproduces the experimental data in the literature for water uptake in Nafion (Figure 3a).[30,33,48,53,54,73-75] Using cylindrical water domains for the swelling pressure formulation (i.e., $n = 2$ in Eq. [8]) results in higher water uptake than the spherical water domains ($n = 3$) at a given humidity. This is due to the fact that the pressure

required to deform the polymer backbone around a spherical domain is higher. As the model is based on a uniform distribution of water domains, the model generates an upper and a lower bound for water uptake, which enclose the measured data (Figure 3a). The membrane has probably a random distribution of spherical domains and cylindrical domains (or channels) and the fraction of cylindrical domains increases with water-uptake due to the expansion of interconnecting channels.[76] Thus, close to saturation, the predictions for the upper bound are consistent with the measured water content.

Overall the good agreement between the model predictions and the experimental data for water uptake validates the theoretical approach which uses only the geometry-dependent swelling pressure function and one fitting parameter, which is the polymer/water interaction energy. Next, we develop the expression to account for compression by changing only the pressure term in the above formulations, which is based on the deformation of the nanostructure and does not require any additional fitting parameter.

Accounting for Compression

Since the thermodynamic equilibrium is always maintained even with constraints on the membrane as discussed by Weber and Newman,[1] equilibrium swelling of a compressed membrane can be written by modifying the pressure term in the chemical potential of water inside the polymer in Eq. [1],

$$\mu_{\mathrm{w}}^{p,c} = RT \ln a_{\mathrm{p}} + \overline{V}_{\mathrm{w}} \Pi\left(p_s, p_e\right) \qquad [11]$$

The new pressure term becomes a function of the original swelling pressure, p_s , and the applied external pressure, p_e . To solve the equation above the functional relationship for the swelling pressure must be determined.

Let a macroscopic cubic volume (V) of membrane be in equilibrium with the environment at water activity a_{w} and temperature T with an equilibrium water content λ . When the membrane is subjected to hydrostatic pressure, i.e. all faces of the volume are subjected to the same pressure, p_e, the new volume becomes $V_c = V - dV$ (Fig. 1). The relationship between the external hydrostatic pressure, p_e, and the resulting volume change (dV) is

$$\frac{dV}{V} = \frac{dV}{V(\phi_{\mathrm{w}})} = \frac{p_e}{K_b(\phi_{\mathrm{w}})} \qquad [12]$$

where we define the pressure as positive and K_{b} is the effective bulk modulus of the membrane that depends on the water volume fraction of the membrane, ϕ_{w} . The bulk modulus of the swollen membrane can determined from the Mori-Tanaka model for two-phase materials,[77]

$$K_b(\phi_{\mathrm{w}}) = K_{\mathrm{pm}} + \phi_{\mathrm{w}} \frac{\left(K_{\mathrm{w}} - K_{\mathrm{pm}}\right)}{1 + (1-\phi_{\mathrm{w}})\left(\dfrac{K_{\mathrm{w}} - K_{\mathrm{pm}}}{K_{\mathrm{w}} + \frac{4}{3} G_{\mathrm{pm}}}\right)} \qquad [13]$$

where K_{pm} and G_{pm} are the bulk and shear modulus of the polymer matrix, respectively, and K_{w} is the bulk modulus of water. Our measurements for the bulk modulus of the membrane using the compression setup (Figure 2) give values of 1.2 to 1.4 GPa for the dry membrane, which is lower than the bulk modulus of water (2.2 GPa).[78] Thus, water-swollen hydrophilic domains act as

reinforcement and therefore the bulk modulus of the swollen membrane should increase with increasing water content.

Alternatively, the bulk modulus can be related to the Young's modulus, *E*, of the material,

$$K_b = \frac{E}{3(1-2\nu)} \qquad [14]$$

where ν is Poisson's ratio, a measure of compressibility. When the compressibility of a material decreases, the bulk modulus approaches infinity and ν approaches 0.5. Young's modulus of Nafion has been measured to be about 250 and 100 MPa for dry and liquid-equilibrated membranes, respectively.[79] Hence, solving Eq. [14] for ν gives values of approximately $\nu = 0.45$ and 0.49 for dry and liquid-equilibrated membranes, respectively. An increase in Poisson's ratio with water uptake means a decrease in compressibility of the membrane, which is consistent with arguments based on Eq. [13] due to the increasing fraction of less compressible water phase.

To determine the compressed-membrane water content, λ_c, more information is needed pertaining the deformation of the microscopic volume, $\hat{V}$, containing the water domains (Figure 1). Change in microscopic volume upon compression, $d\hat{V}$, can be written in terms of changes in *d*-spacing in three (x, y, z) directions,

$$\frac{\hat{V}_c}{\hat{V}} = 1 - \frac{d\hat{V}}{\hat{V}} = \frac{d_x^c}{d_x}\frac{d_y^c}{d_y}\frac{d_z^c}{d_z}, \qquad [15]$$

where the volume change can be related to the externally applied pressure,

$$\frac{d\hat{V}}{\hat{V}} = k_c \frac{p_e}{K_b(\phi_w)} \qquad [16]$$

where k_c is the proportionality constant for compressive deformation, similar to the swelling ratio defined earlier in Eq. [7]. For $k_c = 1$, the macroscopic and microscopic volume changes are the same ($d\hat{V}/\hat{V} = dV/V$), and Eqs. [12] and [16] reduce to the same form. However, our findings indicate that this is not the case for Nafion membranes, where Eq. [16] is validated by our SAXS data for the *d*-spacing of a compressed membrane in three directions, which suggest a strong linear relationship with a slope, k_c, of 7 ± 1.5.[80] This slope is much higher than unity suggesting that there is some kind of morphological change that occurs under mechanical loads and which results in the hydrophilic domains coming closer together, similar to the high value seen with water uptake discussed above. The exact nature of this change is not entirely known, but it is probably similar to the polymer chains lying down and the domains becoming more cylindrical or lamellar rather than spherical, a phenomenon explored in analyzing stretched Nafion membranes.[12,42,81]

The swelling pressure in Eq. [8] can now be rewritten by adding a term for the additional change in *d*-spacing due to the compression

$$\frac{p_s^{\mathrm{c}}}{E_{\mathrm{pm}}} = 1 - \frac{d_{\mathrm{c}}}{d}\frac{d}{d_{\mathrm{dry}}}\left(\frac{1-\phi_{\mathrm{pore}}{}^{1/n}}{1-\phi_{\mathrm{pore}}^{\mathrm{dry}\,1/n}}\right), \qquad [17]$$

where

$$\frac{d_{\mathrm{c}}}{d} = \left(\frac{\hat{V}_{\mathrm{c}}}{\hat{V}}\right)^{1/3} = \left(1 - k_c\frac{p_e}{K_b}\right)^{1/3}. \qquad [18]$$

Note that $d_{\mathrm{c}}/d = 1$ in the absence of external pressure ($p_e = 0$), and the original expression for the swelling pressure (Eq. [8]) is recovered since deformation of the polymer matrix is due

entirely to the growth of the hydrophilic domains during water uptake for this case. Moreover, examination of the equations shows that the effect of compression is predicted to be not significant at low water contents where the swelling pressure is low ($p_s / E_{\text{pm}} << 1$) or at low external pressures ($p_e / K_b << 1$).

Predicting the Water Content and Transport Properties

The model determines the water content, λ, as a function of external water activity or relative humidity (RH), temperature (T), and externally applied pressure (p_e). The solution procedure can be summarized as follows:

$$\begin{array}{c} \chi(T,\lambda) \\ a_w, T \rightarrow \Pi(T,\lambda) \Leftrightarrow \lambda \\ E_{\text{pm}}(T) \\ \uparrow \\ p_e \end{array} \qquad [19]$$

It should be noted that the only fitting parameter is the polymer/water interaction energy, which is fit to the water-uptake data without compression or constraint. By solving Eq. [6] for water content, λ, using the proposed swelling pressure function (Eq. [17]), the relative decrease in water content of a compressed membrane, λ_c/λ, at a given temperature and RH can be determined as a function of pressure.

It is known that the transport properties (e.g., water diffusivity and ionic conductivity) of PFSA membranes are highly dependent on their water content. Thus, once the water content of a compressed membrane is determined, its transport properties can also be estimated from expressions in literature[49], for example, conductivity is

$$\kappa(\phi_{\mathrm{w}},T)=0.5\left(\phi_{\mathrm{w}}-0.06\right)^{1.5}\exp\left[\frac{15000}{R}\left(\frac{1}{T}-\frac{1}{298}\right)\right]\ \text{[S/cm]} \qquad [20]$$

where the water volume fraction can be written in terms of water content and pressure,

$$\phi_{\mathrm{w}}(p_e,\lambda)=\frac{\lambda\bar{V}_{\mathrm{w}}}{\lambda\bar{V}_{\mathrm{w}}+\left(1-\frac{p_e}{K_{\mathrm{p}}}\right)\bar{V}_{\mathrm{p}}}. \qquad [21]$$

In determining the water volume fraction, the change in the molar volume of the polymer backbone due to the applied pressure is also considered. With increasing pressure, the volume of the polymer backbone also decreases resulting in a lower $\bar{V}_{\mathrm{p}}$. Since the molar volume is related to the polymer's EW and dry density, Eq. [4], the compression effect can be interpreted as increasing the density of the polymer backbone. However, this compression-induced volume change is small for the pressure range of interest in this work. If the bulk modulus of the backbone can be assumed to be similar to that of a dry PFSA polymer, which is 1.2 to 1.5 GPa, creating 1% volume change requires the pressure to be more than 12 MPa (see Eq. [12]). Furthermore, the use of the literature expressions for the transport properties assumes that the mechanism in both the compressed and uncompressed membranes is the same and just a function of water volume fraction, which is probably valid as a first estimation since transport-property data on compressed membranes is lacking.

Swelling of a Constrained Membrane

Another interesting case is the swelling of a constrained membrane in which the pressure is developed implicitly as a result of the swelling rather being externally applied as for the

compressed membrane (Figure 1). For a dry membrane that is constrained along its edges, upon exposure to humidity it swells freely in the thickness direction by absorbing water while not be allowed to swell in plane, thereby causing pressure in the plane of the membrane. The pressure arising from this swelling strain can be determined as

$$p_{\text{in-plane}} = \frac{E}{1-\nu}\varepsilon_{\text{in-plane}} = \frac{E}{1-\nu}\left(\phi_{\text{p}}^{-1/3} - 1\right). \quad [22]$$

where the swelling strain is written as a function of the polymer volume fraction. Also, the change in Young's modulus of the membrane during water uptake can be estimated as $E = E_{\text{pm}}\phi_{\text{p}}^{3.6}$ (for details see reference [82]). Thus, Eq. [22] becomes

$$\frac{p_{\text{in-plane}}(\phi_{\text{p}})}{E_{\text{pm}}} = \frac{1}{1-\nu}\phi_{\text{p}}^{3.6}\left(\phi_{\text{p}}^{-1/3} - 1\right), \quad [23]$$

and the total swelling pressure term takes the form

$$\frac{\Pi_s}{E_{\text{pm}}} = \frac{p_s}{E_{\text{pm}}} + \frac{1}{1-\nu}\phi_{\text{p}}^{3.6}\left(\phi_{\text{p}}^{-1/3} - 1\right). \quad [24]$$

Note that there is no explicit pressure term for the external compression in Eq. [24], unlike the compression case (Eq. [17]). Instead, the pressure develops during the swelling of constrained membrane and is calculated simultaneously while solving for the water content using Eq. [6].

Alternatively, if one assumes that the nanostructural reorganization occurring under compression takes place for a constrained membrane too, then using Eq. [17] by replacing the external pressure term with the in-plane pressure term in Eq. [23] (i.e., $p_{\text{e}} = p_{\text{in-plane}}$) gives another solution. Interestingly, the results obtained using this approach are very similar to those obtained using Eq. [24] and therefore will not be discussed further.

Results and Discussion

Water Uptake of Compressed Membranes

The above model is validated through different experimental data based on in- and ex-situ compression tests and in-situ neutron imaging from literature. The experimental data from the in-situ compression test of liquid-equilibrated membranes are summarized in Figure 4. The measured change in water content, λ_c / λ, as a function of applied pressure is plotted in the figure along with our model predictions based on the modified swelling pressure. Experimental data from Budinski and Cook[21] are also included in the figure. The test setup (Figure 2) creates an almost hydrostatic compression condition; therefore the measured applied pressure is adjusted to represent the hydrostatic pressure for consistency with the model predictions (see Appendix). There is good agreement between the theory and experiments which shows that water content decreases with increasing pressure in a highly nonlinear fashion.

Eq. [8] suggests that for a highly swollen membrane ($\phi_w \cong 0.25$), the swelling pressure is between 20 and 25 MPa, which is higher than the cell assembly pressures (1 to 3 MPa), but within the same order of magnitude with the measured values in this work and in the literature.[21-23] The consistency between the measured and calculated pressure values also lend credence to the modeling approach taken.

To understand better the effect of nanostructure on the results, model predictions for k_c =1 (Eq. [16]) are shown in the figure. It follows from the figure that ignoring the nanoscale deformation underestimates the water loss. When the deformation of the nanostructure is

characterized based on the measured value (k_c = 7.5), the model and data come into agreement. In addition, setting $k_c = k_s$ = 5.6, i.e. the swelling ratio defined in Eq. [7], also provides a good prediction. The predictions of the model using the swelling-pressure function Eq. [17] for various k_c values will be referred to as "deformation-based". Thus, the compression mechanism of polymer-backbone deformation during swelling and under compression might be similar as structural reorganization occurs in both cases. Our findings suggest that the swelling process in ionomer membranes is a multiscale phenomenon and the effect of compression must be considered at all relevant lengthscales.

The proposed model relies on knowledge of the multiscale morphological changes under mechanical and swelling loads. If this information is unavailable, a simpler approach can be taken by assuming that the applied pressure is the same throughout the polymer/water network at all scales. This assumes a uniform distribution of hydrostatic pressure in the polymer matrix and represents the case of a severe constraint. For this case, the applied external pressure is added directly to the swelling pressure expression (Eq. [8]).

$$\Pi_s(\phi_w) = p_s(\phi_w) + p_e \,. \qquad [25]$$

When Eq. [25] is used, the model predicts the largest water loss and creates a lower bound for the measured data. This case will be referred to as "pressure-based" as no information on the deformation of the nanostructure (i.e., k_c) is needed. Figure 4 demonstrates that the measured data falls between the envelope generated by the deformation-based model (Eq [17], upper bound) and pressure-based model (Eq. [25], lower bound). The difference between the two approaches can be attributed to the type of the constraint to which membrane is subjected. For

example, thickness compression of the membrane (in one direction) is less severe than pure hydrostatic compression of the membrane (in all directions). However as the membranes are not under pure hydrostatic compression in most real applications, the deformation-based modeling approach provides a flexible tool to investigate other types of constraints by varying the parameter k_c.

For further validation, the model was fit to data from Los Alamos National Lab[17] which determined the in-situ water content of a membrane for various stack compression loads as shown in Figure 5. To visualize the compression effect better, the water content of the compressed membrane (3 MPa), λ_c, is normalized to that for low compression case (λ_c / λ) and plotted as a function of RH (Figure 5B). The model predictions agree well with the data suggesting a decrease in water content especially when the membrane is liquid-equilibrated. At low humidities (RH < 90%), however, the compression effect is negligible for the level of pressures (< 3 MPa) investigated in accord with model predictions.

To investigate explicitly the effect of compression on the swelling of the membrane alone, we used a setup to measure the water loss of a membrane compressed between aluminum plates using neutron radiography. Images taken for both the face-on (surface) and edge-on (thickness) directions are shown in Figure 6 for dry, liquid-equilibrated (wet), and compressed wet samples. When the wet samples were compressed, water pools around the membrane were observed indicating water loss (Figure 6C). The change in the area and thickness of the wet samples before and after compression are also determined from the images. Interestingly, surface area of the samples does not change upon compression (Figure 6B-C), at least for these compression

levels and experimental resolutions. However, the thickness of the wet samples clearly decreases upon compression (Figure 7A), which indicates that de-swelling of the membrane is driven by the compressive thickness reduction.

In addition, Figure 7 shows the water content of the uncompressed and compressed membrane estimated from the sample dimensions in the radiographs. For example, λ decreases from 15±1 to 13±1.5[§] upon compression. Also, the water content for the (uncompressed) wet sample determined from a gravimetric method is in accord with those determined from the neutron radiographs (Figure 7B). Thus, we can rely on the neutron-imaging data to estimate the water content of the compressed wet samples. Overall, λ decreases by 10 to 15% for the pressure range of 2 to 4 MPa, and up to 70 to 90% of this water loss was observed in the form of water droplets around the edges of the samples.

Also included in Figure 7B is the water content of a "pre-constrained" membrane. In this case, the as-received sample was clamped between plastic plates and allowed to equilibrate in DI water for 1 day. Then, the image of the membrane alone was taken without external compression even though the membrane develops internal pressure from swelling similar to the constrained case discussed above. The water content also decreases in this case, although a lot of water was still absorbed. For the pre-constrained membrane, the thickness is almost the same as the wet membrane (Figure 7A) but the area decreases, the exact opposite of what we observed for the compressed membranes. Thus, de-swelling of the membrane in the thickness and in-plane

[§] Relatively large error in the estimated water content is due to the limited resolution of neutron radiographs and variation in the swelling of the samples.

directions differ significantly depending on whether the membrane is compressed or pre-constrained.

The water content of vapor- and liquid-equilibrated membranes obtained from the two different experiments are shown together in Figure 8 along with the model predictions. The model can successfully predict the effect of pressure, phase of water, and temperature on water content with no additional fitting parameters beyond that used to fit the uncompressed water-uptake isotherm. The results show that water uptake decreases for vapor-equilibrated membrane when the temperature is increased to 80°C from 25°C. In addition, liquid-equilibrated-membrane water uptake at 80°C is much larger than that of the vapor-equilibrated membrane. This is because when the membrane is in liquid water the interaction parameter becomes temperature-independent ($\chi_T = 0$ in Eq. [5]). In addition, there is a decrease in backbone modulus of the membrane with temperature (e.g., $E_{\mathrm{pm}}(80) < E_{\mathrm{pm}}(25)$), which also reduces pressure exerted by the polymer backbone to the water domains. Moreover, the model predictions are extended up to 25 MPa which shows that the decrease in water content becomes less significant at higher pressures.

As the model was successfully validated using the measured data from different experiments, the theory can be used to investigate the effects of pressure on the water-dependent transport properties, such as conductivity. Figure 9 shows how the sorption isotherms of Nafion® membrane at 25°C changes with the applied pressure. The decrease in water content due to the hydrostatic compression is less than 5% for relative humidities lower than 60%, whereas the decrease could be as high as 20% at higher relative humidities (> 80% RH) for the pressure

range of 5 to 10 MPa. Since most PEFCs operate with bolt pressures around 2 to 5 MPa, it is expected that compression does not have a major impact on membrane water content for most operating conditions, and in fact compression probably impacts contact resistance more significantly then membrane water content.[17]

Water Uptake of a Constrained membrane

The predicted equilibrium water content of a vapor-equilibrated membrane constrained along its edges is plotted in Figure 10 as a function of water activity. The constraint is implemented such that the membrane cannot expand in the plane but is free to expand in the thickness direction. Constraining the membrane decreases the water content from 14 to 10 at saturation (100% RH), whereas constraining is less effective at reducing the water-uptake at humidities below 70%. Moreover, compared to 25°C the effect of constraint on water uptake is less pronounced at 85°C. This change is due to the decrease in the membrane's Young's modulus with increasing temperature. Notice that for the case of compression, the externally applied pressure is independent of Young's modulus and temperature, whereas the pressure (compressive stress) generated in the constrained membrane becomes a function of Young's modulus (see Eq. [24]). Hence, a lower Young's modulus reduces the compressive stress developed during swelling and therefore reduces the impact of constraint on water uptake. Figure 10 also shows that water content of liquid-equilibrated PFSA membrane at 85°C decreases by 10% when the membrane is constrained. The relatively smaller decrease in λ for this case compared to the vapor-equilibrated membrane is due to low Young's modulus of the membrane at higher temperatures.

The relatively high water uptake of a constrained membrane in liquid water indicates that the membrane, when it is free to expand in the thickness direction, could easily overcome the constraining pressure and absorb water. Therefore, constraining the membrane in one direction does not cause a big decrease in water content as does hydrostatically compressing the membrane (see, for example, Figure 8). Lastly, another interesting aspect of the constraint condition is that even though the total water content decreases with constraint, the constrained membrane actually swells more in the thickness direction than an unconstrained membrane which swells in all directions.

Effect of compression on conductivity

The protonic conductivity of the compressed membrane can be predicted using the above model and Eq. [20]. The calculated values are shown in Figure 11 as a function of RH at selected pressures. As the water content decreases with increasing pressure, the conductivity of the membrane also reduces with increasing level of compression. This stems from the fact that the water volume fraction within the membrane decreases with compression, which demonstrates that the water content decreases faster than the volume of the membrane, in contradiction to the discussion of Weber and Newman[1] who used a more simplistic approach. Moreover, if one assumes that conductivity is directly proportional to the water content ($\kappa \propto \lambda$) then the decrease in conductivity would be more significant compared to the water-volume-fraction dependent conductivity (see Eq. [21]). The model predictions suggest that conductivity could decrease under high pressures for fully vapor-equilibrated membranes whereas the effect of compression both on water content and conductivity is almost negligible for RHs less than 70%.

The effect of temperature is also shown in Figure 11. Since the effect of pressure on water content becomes less significant at higher temperatures (see Figure 8), the conductivity of the highly compressed membrane at 85°C is still much higher than that of an uncompressed membrane at 25°C. Thus, it is fair to say that temperature has a more important role than the pressure in controlling the conductivity of the membrane.

Furthermore, when the membrane is subjected to hydrostatic compression the change in conductivity is isotropic. However, other deformation modes, such as uniaxial compression or tension or even constraint, could generate anisotropy due to the orientation of the polymer backbone where the conductivity would be dependent on the anisotropic changes in *d*-spacing in addition to the compression (or tension) load.

Summary

In this paper, the effect of compression on the water-uptake behavior of polymer-electrolyte-fuel-cell membranes was investigated through theoretical and experimental means. A multiscale modeling framework using electrochemical equilibrium and polymer physics was developed to predict water uptake at different relative humidities and temperatures using only one fitting parameter, the polymer/water interaction energy. This methodology was modified by changing the swelling pressure term in the thermodynamic equilibrium to account for the deformation of the polymer backbone due to (i) the growth of water domains during swelling, and (ii) the externally applied pressure. The latter effect is implemented as a change in the nanoscale domain spacing of the compressed membrane. In this fashion, the model was able to predict the impact

of compression and constraint on water content. The model was validated and shown to be in good agreement with membrane water-content data under hydrostatic compression and in- and ex-situ water-uptake measurements as a function of applied pressure using neutron imaging. Thus, an accurate model for swelling under external loads requires characterization of the growth of water domains and associated backbone deformation at both the nanoscopic and microscopic lengthscales. It is this multiscale deformation phenomenon that generates the high swelling pressures in the polymer backbone during water uptake even for an uncompressed membrane. The results suggest that constraining and/or compressing the membrane might reduce its average water content and consequently its conductivity, especially at higher humidities, lower temperatures, and in liquid water. In general, the model demonstrates that water uptake is limited dramatically under high pressures (> 10 MPa) resulting in lower transport properties such as conductivity, although further increases in pressure result in diminishing impact. The model and results have implications and applicability for ionomers used in many devices including fuel cells and batteries. However, under typical fuel-cell operating conditions and cell-assembly pressures, the impact of compression and constraint on performance is not expected to be as significant as other compression-related issues (e.g., contact resistance).

Acknowledgements

This work was funded by the Assistant Secretary for Energy Efficiency and Renewable Energy, Office of Fuel Cell Technologies, of the U. S. Department of Energy under contract number DE-AC02-05CH11231. Additionally, the authors thank Dr. Rodney Borup for helpful discussions.

We would also like to thank Ray Tang, Ron Walker, and Jae-Wan Park of University of California at Davis for their kind help with facilitating the use of equipment at McCellan Nuclear Research Center (MNRC) for the ex-situ water imaging. Lastly, we gratefully acknowledge Craig Gittleman and Yeh-hung Lai of the Electrochemical Energy Research Lab at General Motors for their insightful comments and providing the fixture for the compression experiments.

APPENDIX

Here the average pressure in the membrane during the compression tests (Figure 2) is determined as a function of the applied pressure. The stress-strain relation in the plane of the membrane is

$$\varepsilon_r = \sigma_r - \nu\sigma_r - \nu\sigma_z \,. \tag{A1}$$

where ε_r and σ_r are the radial strain and stress, respectively, and σ_z is the stress in the thickness direction, which is equal to the applied pressure, i.e. $\sigma_z = -p_{\text{applied}}$. As the membrane is constrained in the fixture it does not expand in the plane, and $\varepsilon_r = 0$. Then, from Eq. (A1) the radial stress becomes $\sigma_r = \sigma_z \nu/(1-\nu)$. Finally, the average pressure, which can be interpreted as the hydrostatic pressure, is calculated from the mean stress:

$$p_e = -\sigma_{\text{mean}} = -\frac{1}{3}\left(2\sigma_r + \sigma_z\right) = -\sigma_z \frac{1}{3}\left(\frac{1+\nu}{1-\nu}\right) = p_{\text{applied}} \frac{1}{3}\left(\frac{1+\nu}{1-\nu}\right). \tag{A2}$$

For liquid-equilibrated membrane Eq. (A2) gives $p_e = 0.97\, p_{\text{applied}}$ (with $\nu \approx 0.49$). Thus, by using the above formula, the applied pressure can be used to represent the hydrostatic pressure.

LIST OF SYMBOLS

a_i = activity of species i

d_i = (water) domain spacing of the membrane in direction i, nm

E = Young's modulus of membrane, MPa

E_{pm} = Young's modulus of the polymer backbone phase of the membrane, MPa

EW = equivalent weight of the PFSA polymer, g/mol

K_b = Bulk modulus of membrane, GPa

K_p = Bulk modulus of dry polymer membrane, GPa

k_c = swelling parameter, ratio of changes in macroscopic volume to domain spacing

k_s = compressive deformation parameter

n = dimensionality parameter, see equation [8]

p_s = swelling pressure in the membrane, MPa

p_e = externally applied hydrostatic pressure, MPa

p = pressure, MPa

R = ideal-gas constant, 8.3143 J/mol-K

r = radius of hydrophilic domains, nm

RH = relative humidity, %

T = absolute temperature, K

$\bar{V}_i$ = (partial) molar volume of species i, cm^3/mol

V = Macroscopic volume of the membrane, cm^3

$\hat{V}$ = Microscopic volume of the membrane surrounding the water domains, cm^3

Greek

χ = Flory-Huggins (FH) interaction parameter

χ_S = swelling-dependent component of FH interaction parameter

χ_T = temperature-dependent component of FH interaction parameter

ε_i = strain in direction *i*, cm

ϕ_α = volume fraction phase α in membrane

ϕ'_p = volume fraction polymer phase plus the bound water in membrane

κ = ionic conductivity of membrane, S/cm

λ = water content, moles of water molecules per mole of sulfonic acid sites

λ_c = water content of a compressed membrane

μ_i = electrochemical potential of species i, J/mol

ν = Poisson's ratio

ρ_p = density of dry polymer, g/cm^3

Subscripts/Superscripts

ref = parameter evaluated at the reference conditions

dry = value of the parameter for the dry membrane

pore = hydrophilic pore (water plus the ionic groups)

w = water

p = polymer

c = value of the parameter for the constrained/compressed membrane

REFERENCES

1. A. Z. Weber and J. Newman, *AIChE Journal*, **50**, 3215 (2004).

2. A. Kusoglu, A. M. Karlsson, M. H. Santare, S. Cleghorn and W. B. Johnson, *Journal of Power Sources*, **161**, 987 (2006).

3. A. Kusoglu, M. H. Santare, A. M. Karlsson, S. Cleghorn and W. B. Johnson, *J Electrochem Soc*, **157**, B705 (2010).

4. D. Bograchev, M. Gueguen, J. C. Grandidier and S. Martemianov, *Journal of Power Sources*, **180**, 393 (2008).

5. R. Solasi, Y. Zou, X. Huang, K. Reifsnider and D. Condit, *Journal of Power Sources*, **167**, 366 (2007).

6. Y.-H. Lai, C. K. Mittelsteadt, C. S. Gittleman and D. A. Dillard, *Journal of Fuel Cell Science and Technology*, **6**, 021002 (2009).

7. S. Escribano, J. F. Blachot, M. Etheve, A. Morin and R. Mosdale, *Journal of Power Sources*, **156**, 8 (2006).

8. W. R. Chang, J. J. Hwang, F. B. Weng and S. H. Chan, *Journal of Power Sources*, **166**, 149 (2007).

9. A. Bazylak, D. Sinton, Z. S. Liu and N. Djilali, *Journal of Power Sources*, **163**, 784 (2007).

10. R. Jiang, C. K. Mittelsteadt and C. S. Gittleman, *J Electrochem Soc*, **156**, B1440 (2009).

11. J. A. Elliott, S. Hanna, A. M. S. Elliott and G. E. Cooley, *Macromolecules*, **33**, 4161 (2000).

12. K. M. Cable, K. A. Mauritz and R. B. Moore, *Chemistry of Materials*, **7**, 1601 (1995).

13. A. Kusoglu, Y. Tang, M. Lugo, A. M. Karlsson, M. H. Santare, S. Cleghorn and W. B. Johnson, *Journal of Power Sources*, **195**, 483 (2010).

14. S. Cleghorn, J. Kolde and W. Liu, in *Handbook of Fuel Cells – Fundamentals, Technology and Applications*, V. Wolf, L. Arnold and G. Hubert Editors, John Wiley & Sons, Ltd (2003).

15. Y. Tang, A. Kusoglu, A. M. Karlsson, M. H. Santare, S. Cleghorn and W. B. Johnson, *Journal of Power Sources*, **175**, 817 (2008).

16. D. Spernjak, P. P. Mukherjee, R. Mukundan, J. Davey, D. S. Hussey, D. Jacobson and R. L. Borup, *ECS Transactions*, **33**, 1451 (2010).

17. R. Borup, Water Transport Exploratory Studies, in *DoE 2010 Annual Merit Review Meeting*, available at http://www.hydrogen.energy.gov (2011).

18. V. Freger, *Polymer*, **43**, 71 (2002).

19. A. Kusoglu, M. H. Santare and A. M. Karlsson, *Polymer*, **50**, 2481 (2009).

20. K. A. Mauritz and C. E. Rogers, *Macromolecules*, **18**, 483 (1985).

21. M. K. Budinski and A. Cook, *Tsinghua Science & Technology*, **15**, 385 (2010).

22. M. Escoubes, M. Pineri and E. Robens, *Thermochim Acta*, **82**, 149 (1984).

23. K. K. Pushpa, D. Nandan and R. M. Iyer, *J Chem Soc Farad T 1*, **84**, 2047 (1988).

24. I. Nazarov and K. Promislow, *J Electrochem Soc*, **154**, 623 (2007).

25. P. J. Flory, *Principles of polymer chemistry*, p. 672, Cornell University Press, Ithaca (1953).

26. F. Horkay and B. McKenna, in *Physical Properties of Polymers Handbook*, J. E. Mark Editor, p. 497, Springer, New York (2007).

27. W. Hong, Z. S. Liu and Z. G. Suo, *International Journal of Solids and Structures*, **46**, 3282 (2009).

28. R. Marcombe, S. Q. Cai, W. Hong, X. H. Zhao, Y. Lapusta and Z. G. Suo, *Soft Matter*, **6**, 784 (2010).

29. X. M. Li, Z. Shen, T. He and M. Wessling, *J Polym Sci Pol Phys*, **46**, 1589 (2008).

30. T. A. Zawodzinski, C. Derouin, S. Radzinski, R. J. Sherman, V. T. Smith, T. E. Springer and S. Gottesfeld, *J Electrochem Soc*, **140**, 1041 (1993).

31. M. Fujimura, T. Hashimoto and H. Kawai, *Macromolecules*, **15**, 136 (1982).

32. G. Gebel and J. Lambard, *Macromolecules*, **30**, 7914 (1997).

33. P. J. James, J. A. Elliott, T. J. McMaster, J. M. Newton, A. M. S. Elliott, S. Hanna and M. J. Miles, *Journal of Materials Science*, **35**, 5111 (2000).

34. A. Gruger, A. Regis, T. Schmatko and P. Colomban, *Vibrational Spectroscopy*, **26**, 215 (2001).

35. B. Dreyfus, G. Gebel, P. Aldebert, M. Pineri, M. Escoubes and M. Thomas, *Journal De Physique*, **51**, 1341 (1990).

36. E. J. Roche, M. Pineri and R. Duplessix, *J Polym Sci Pol Phys*, **20**, 107 (1982).

37. M. Laporta, M. Pegoraro and L. Zanderighi, *Physical Chemistry Chemical Physics*, **1**, 4619 (1999).

38. T. D. Gierke, G. E. Munn and F. C. Wilson, *Journal of Polymer Science, Polymer Physics Edition*, **19**, 1687 (1981).

39. M. H. Kim, C. J. Glinka, S. A. Grot and W. G. Grot, *Macromolecules*, **39**, 4775 (2006).

40. K. Schmidt-Rohr and Q. Chen, *Nature Materials*, **7**, 75 (2008).

41. H. G. Haubold, T. Vad, H. Jungbluth and P. Hiller, *Electrochimica Acta*, **46**, 1559 (2001).

42. L. Rubatat, A. L. Rollet, G. Gebel and O. Diat, *Macromolecules*, **35**, 4050 (2002).

43. F. P. Orfino and S. Holdcroft, *Journal of New Materials for Electrochemical Systems*, **3**, 285 (2000).

44. G. Gebel, *Polymer*, **41**, 5829 (2000).

45. G. Meresi, Y. Wang, A. Bandis, P. T. Inglefield, A. A. Jones and W. Y. Wen, *Polymer*, **42**, 6153 (2001).

46. E. J. Roche, M. Pineri, R. Duplessix and A. M. Levelut, *J Polym Sci Pol Phys*, **19**, 1 (1981).

47. Y. Termonia, *Polymer*, **48**, 1435 (2007).

48. P. Choi, N. H. Jalani and R. Datta, *Journal of the Electrochemical Society*, **152**, E123 (2005).

49. A. Z. Weber and J. Newman, *J Electrochem Soc*, **151**, 311 (2004).

50. W. Y. Hsu and T. D. Gierke, *Macromolecules*, **15**, 101 (1982).

51. B. Dreyfus, *J Polym Sci Pol Phys*, **21**, 2337 (1983).

52. A. Eisenberg, *Macromolecules*, **3**, 147 (1970).

53. P. H. Choi and R. Datta, *J Electrochem Soc*, **150**, E601 (2003).

54. H. Takata, N. Mizuno, M. Nishikawa, S. Fukada and M. Yoshitake, *International Journal of Hydrogen Energy*, **32**, 371 (2007).

55. E. L. Thompson, T. W. Capehart, T. J. Fuller and J. Jorne, *J Electrochem Soc*, **153**, A2351 (2006).

56. A. Siu, J. Schmeisser and S. Holdcroft, *Journal of Physical Chemistry B*, **110**, 6072 (2006).

57. M. Saito, K. Hayamizu and T. Okada, *Journal of Physical Chemistry B*, **109**, 3112 (2005).

58. P. Futerko and I. M. Hsing, *J Electrochem Soc*, **146**, 2049 (1999).

59. R. S. Yeo, *Polymer*, **21**, 432 (1980).

60. C. M. Gates and J. Newman, *AIChE Journal*, **46**, 2076 (2000).

61. J. T. Hinatsu, M. Mizuhata and H. Takenaka, *J Electrochem Soc*, **141**, 1493 (1994).

62. G. Alberti and R. Narducci, *Fuel Cells*, **9**, 410 (2009).

63. F. M. Collette, C. Lorentz, G. Gebel and F. Thominette, *Journal of Membrane Science*, **330**, 21 (2009).

64. M. J. Park, K. H. Downing, A. Jackson, E. D. Gomez, A. M. Minor, D. Cookson, A. Z. Weber and N. P. Balsara, *Nano Lett*, **7**, 3547 (2007).

65. S. Y. Kim, M. J. Park, N. P. Balsara and A. Jackson, *Macromolecules*, **43**, 8128 (2010).

66. M. J. Park, N. P. Balsara and A. Jackson, *Macromolecules*, **42**, 6808 (2009).

67. P. M. Mangiagli, C. S. Ewing, K. Xu, Q. Wang and M. A. Hickner, *Fuel Cells*, **9**, 432 (2009).

68. L. M. Onishi, J. M. Prausnitz and J. Newman, *Journal of Physical Chemistry B*, **111**, 10166 (2007).

69. E. L. Thompson, J. Jorne, W. B. Gu and H. A. Gasteiger, *J Electrochem Soc*, **155**, B625 (2008).

70. M. Bass and V. Freger, *Desalination*, **199**, 277 (2006).

71. G. Alberti, R. Narducci and M. Sganappa, *Journal of Power Sources*, **178**, 575 (2008).

72. W. Y. Hsu and T. D. Gierke, *Journal of Membrane Science*, **13**, 307 (1983).

73. N. H. Jalani and R. Datta, *Journal of Membrane Science*, **264**, 167 (2005).

74. D. R. Morris and X. D. Sun, *Journal of Applied Polymer Science*, **50**, 1445 (1993).

75. S. Ochi, O. Kamishima, J. Mizusaki and J. Kawamura, *Solid State Ionics*, **180**, 580 (2009).

76. A. Z. Weber and J. Newman, *J Electrochem Soc*, **150**, 1008 (2003).

77. Y. Benveniste, *Mechanics Research Communications*, **13**, 193 (1986).

78. D. Halliday, R. Resnick and J. Walker, *Fundamentals of Physics, Chapters 1-20*, John Wiley & Sons (2010).

79. A. Kusoglu, M. H. Santare, A. M. Karlsson, S. Cleghorn and W. B. Johnson, *Journal of Polymer Science Part B: Polymer Physics*, **46**, 2404 (2008).

80. A. Kusoglu, A. Hexemer, J. Ruichun, C. S. Gittleman and A. Z. Weber, *Macromolecules*, in preparation (2011).

81. J. Li, J. K. Park, R. B. Moore and L. A. Madsen, *Nature Materials*, **10**, 507 (2011).

82. A. Kusoglu, A. M. Karlsson and M. H. Santare, *Polymer*, **51**, 1457 (2010).

83. M. Fujimura, T. Hashimoto and H. Kawai, *Macromolecules*, **14**, 1309 (1981).

CAPTIONS

Figure 1 Change in the macroscopic dimensions and domains spacing (at nano length-scales) of a constrained membrane and compressed membrane in a humid environment.

Figure 2 Compression fixture used to determine the swelling pressure of the liquid-equilibrated membrane. The device is attached to a electromechanical testing machine that controls the pressure and records the thickness change.

Figure 3 (a) Model predictions for water-uptake at 25°C compared with measured data from literature.[30,33,48,53,54,73-75] (b) Swelling phenomenon at multiple scales: change in *d*-spacing plotted as a function of macroscopic swelling of the sample based on our measurements and data from the literature.[35,72,83]

Figure 4 Change in water content as a function of pressure at room temperature as predicted from the model compared with measured data and data from Budinski and Cook.[21] Predictions of a simplified macroscopic model (for $k_c = 1$) are also included for comparison.

Figure 5 Water uptake of a compressed membrane determined from neutron imaging of a fuel-cell setup[17] compared with our model predictions: (a) sorption isotherm and (b) normalized water content.

Figure 6 Images taken from the face-on neutron radiographs of (a) dry, (b) liquid-equilibrated "wet" (uncompressed) and (c) compressed wet samples for 1000EW and 1100EW PFSA membrane. Water leaving the compressed samples is highlighted in (c).

Figure 7 Swelling data for 0.750 mm thick PFSA membrane obtained from neutron radiographs of dry, wet and compressed wet membrane: (a) thickness, (b) water content. Actual thickness of the samples and water content from a gravimetric method are also included for comparison.

Figure 8 Model predictions for the effect of pressure on the water content of Nafion® membrane for liquid-equilibrated at 80°C and fully vapor-equilibrated at 25 and 80°C. Measured water contents from in-situ and ex-situ neutron imaging are also shown for each condition. The lines are the upper and lower bound predictons of the model corresponding to the measured compressive deformation-based case ($k_c = 7.5$) and pressure-based case (as shown in Figure 4).

Figure 9 Predicted effect of hydrostatic pressure on the membrane sorption isotherm at 25°C (using the swelling pressure function Eq. [17] with $k_c = 7.5$).

Figure 10 Model predictions for the sorption isotherms of a vapor-equilibrated membrane at 25 and 85°C and water content of a liquid-equilibrated membrane at 85°C when the membrane is unconstrained and constrained. (Constrained membrane cannot expand in the plane but is free to expand in the thickness direction.)

Figure 11 Model predictions for the conductivity of uncompressed and compressed membranes as a function of water activity at 25 and 85°C.

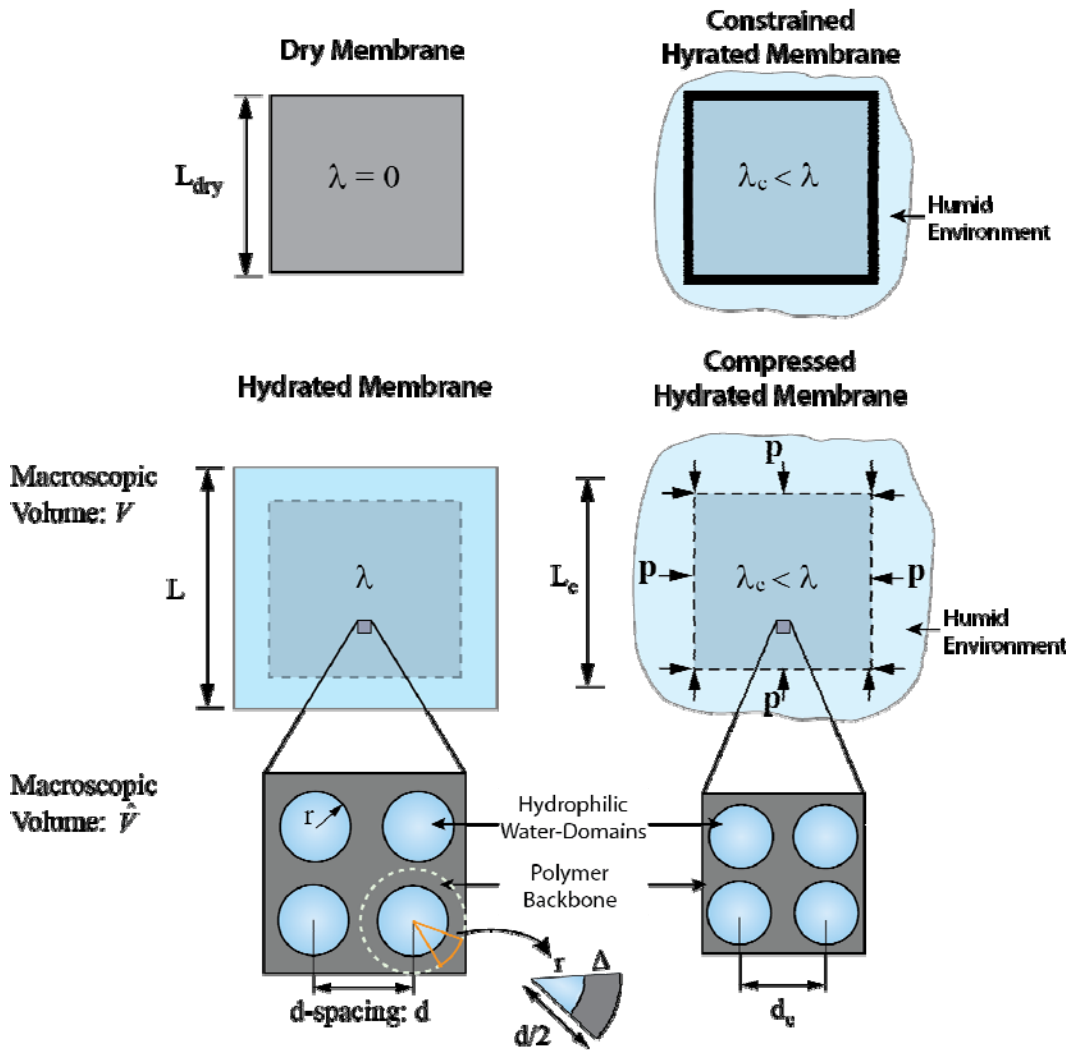

Figure 1 Change in the macroscopic dimensions and domains spacing (at nano length-scales) of a constrained membrane and compressed membrane in a humid environment.

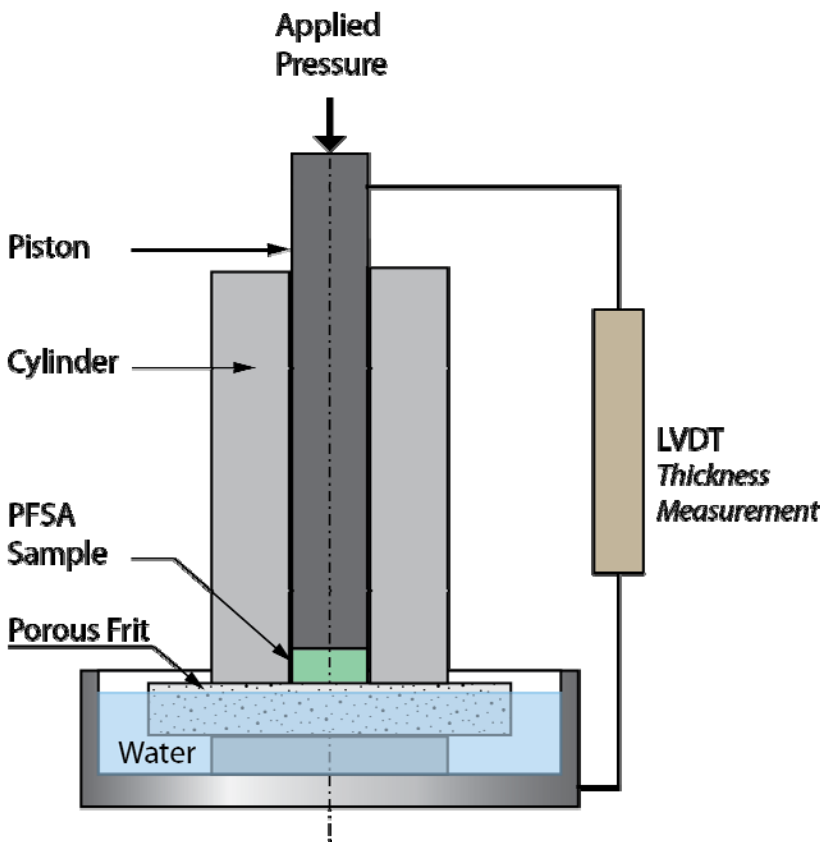

Figure 2 Compression fixture used to determine the swelling pressure of the liquid-equilibrated membrane. The device is attached to a electromechanical testing machine that controls the pressure and records the thickness change.

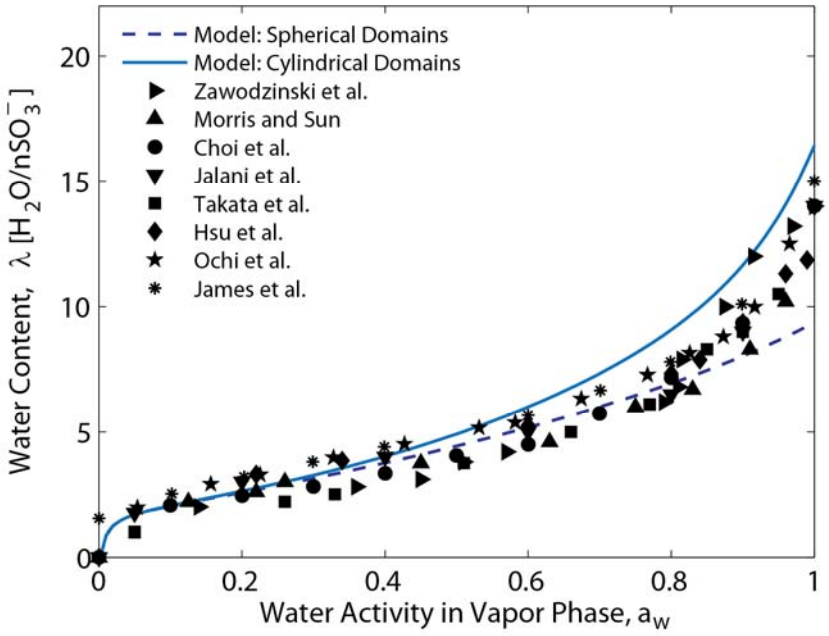

(a)

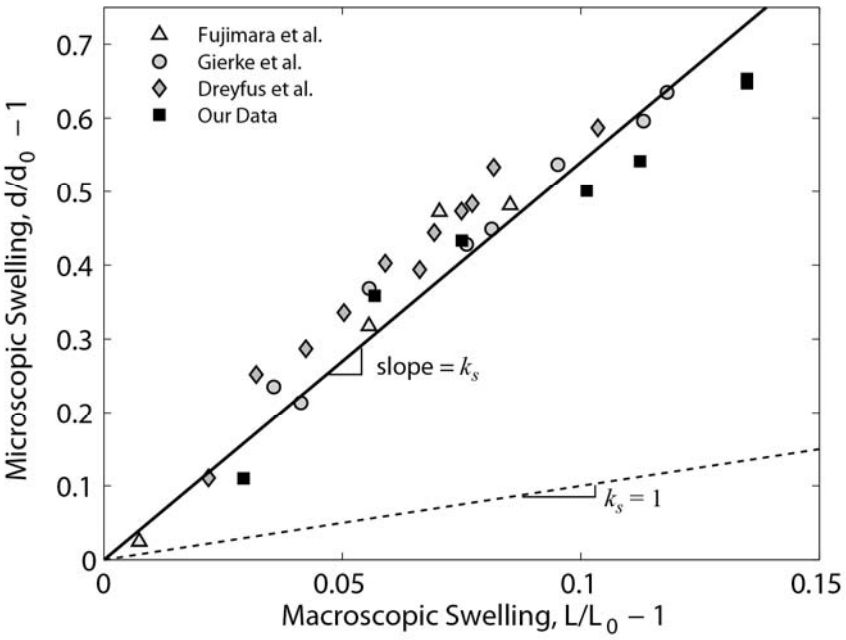

(b)

Figure 3 (a) Model predictions for water-uptake at 25°C compared with measured data from literature.[30,33,48,53,54,73-75] (b) Swelling phenomenon at multiple scales: change in *d*-spacing plotted as a function of macroscopic swelling of the sample based on our measurements and data from the literature.[35,72,83]

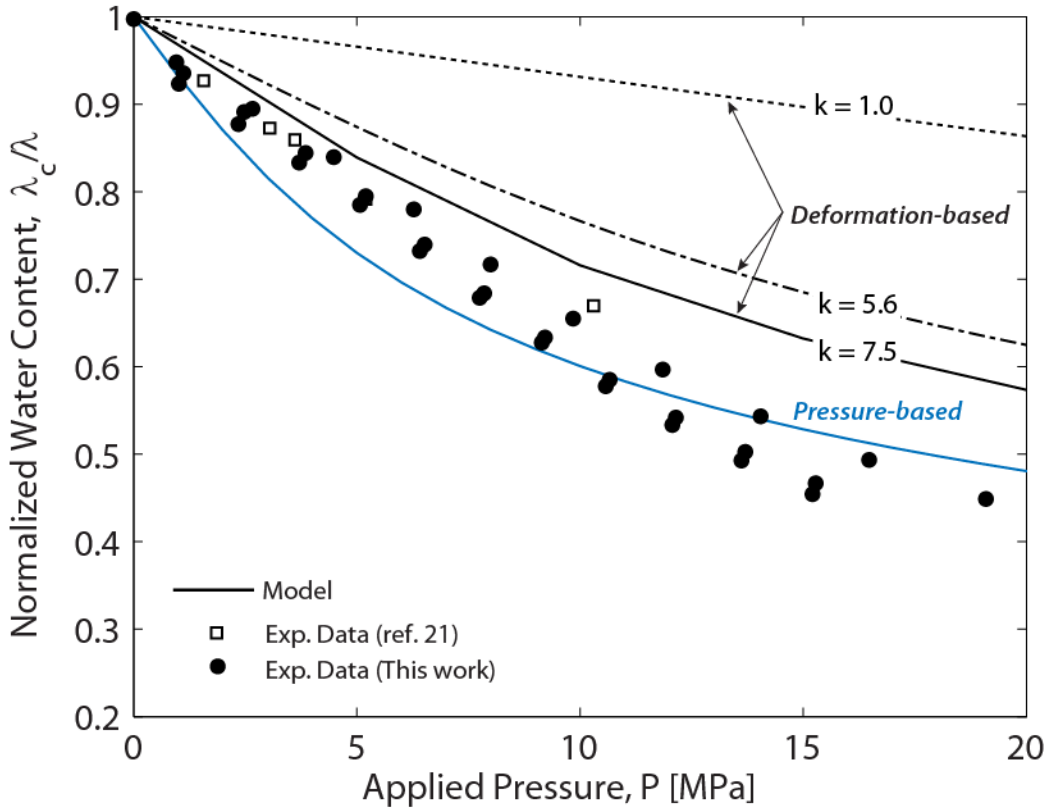

Figure 4 Change in water content as a function of pressure at room temperature as predicted from the model compared with measured data and data from Budinski and Cook.[21] Predictions of a simplified macroscopic model (for k_c = 1) are also included for comparison.

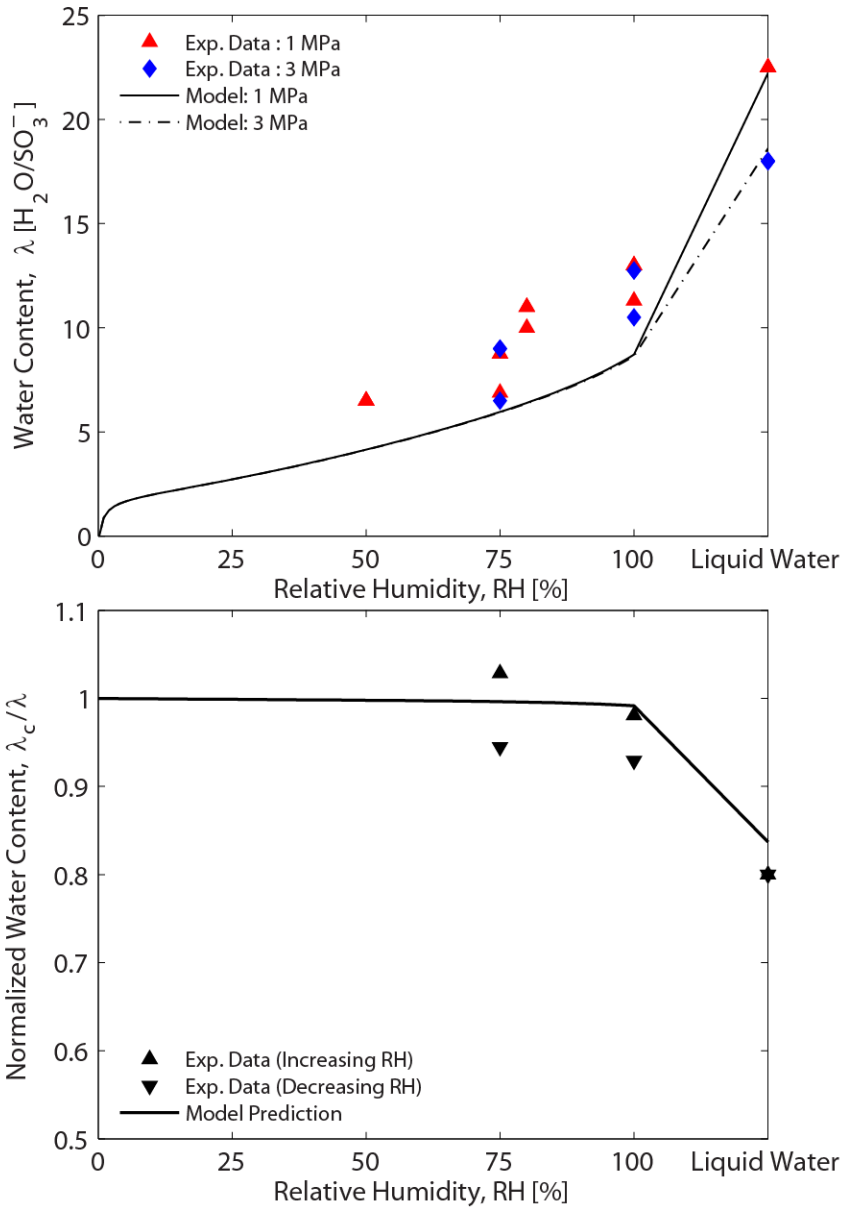

Figure 5 Water uptake of a compressed membrane determined from neutron imaging of a fuel-cell setup[17] compared with our model predictions: (a) sorption isotherm and (b) normalized water content.

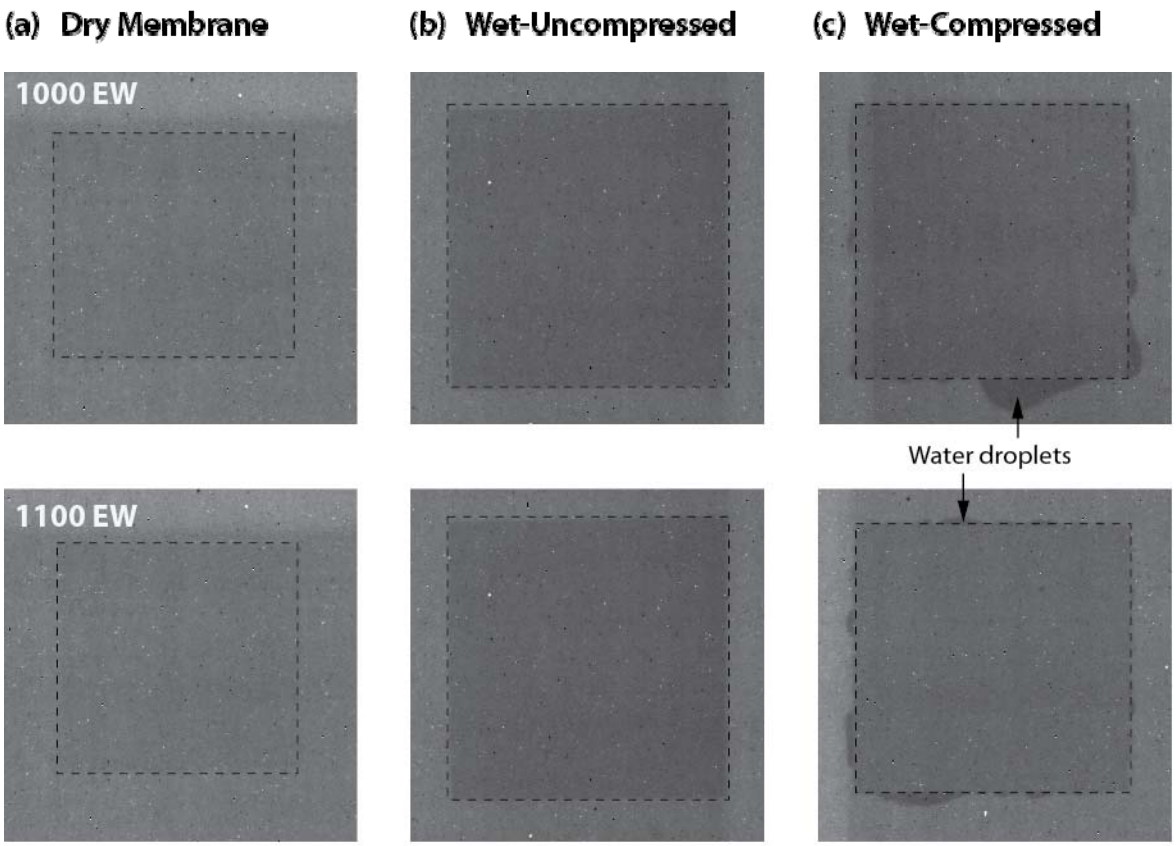

Figure 6 Images taken from the face-on neutron radiographs of (a) dry, (b) liquid-equilibrated "wet" (uncompressed) and (c) compressed wet samples for 1000EW and 1100EW PFSA membrane. Water leaving the compressed samples is highlighted in (c).

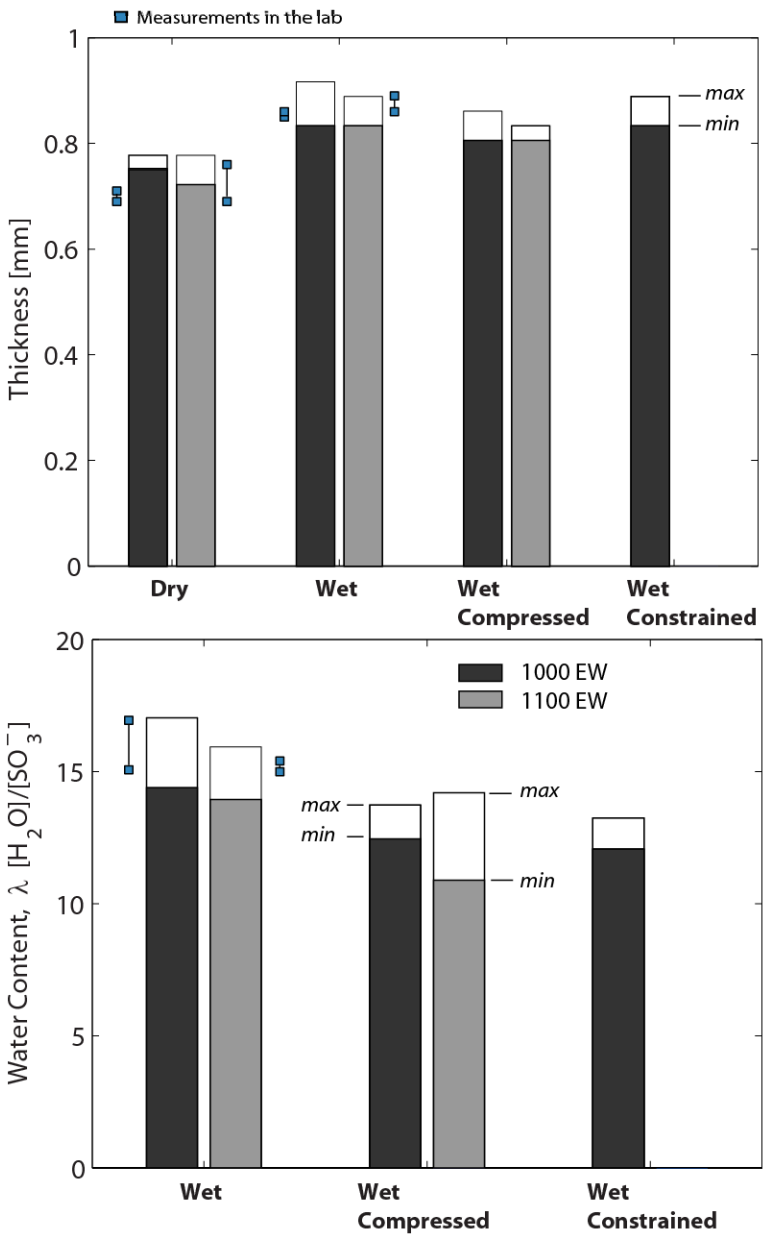

Figure 7 Swelling data for 0.750 mm thick PFSA membrane obtained from neutron radiographs of dry, wet and compressed wet membrane: (a) thickness, (b) water content. Actual thickness of the samples and water content from gravimetric method are also included for comparison.

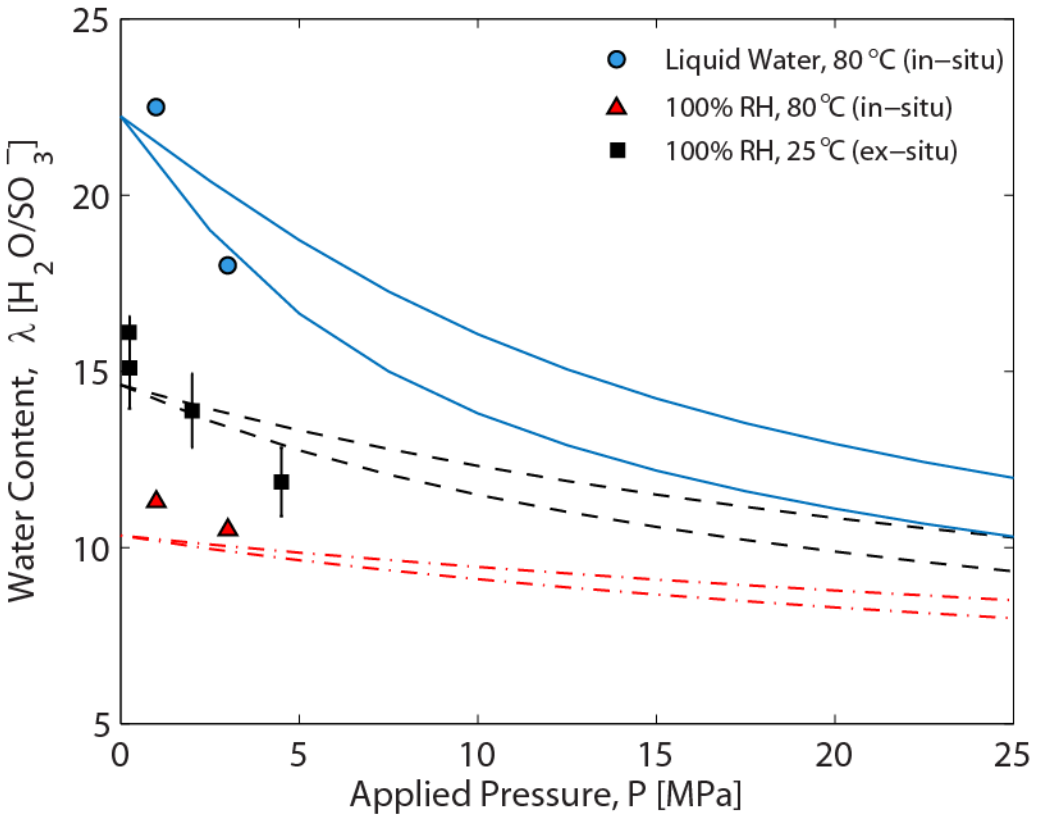

Figure 8 Model predictions for the effect of pressure on the water content of Nafion® membrane for liquid-equilibrated at 80°C and fully vapor-equilibrated at 25 and 80°C. Measured water contents from in-situ and ex-situ neutron imaging are also shown for each condition. The lines are the upper and lower bound predictons of the model corresponding to the measured compressive deformation-based case (k_c = 7.5) and pressure-based case (as shown in Figure 4).

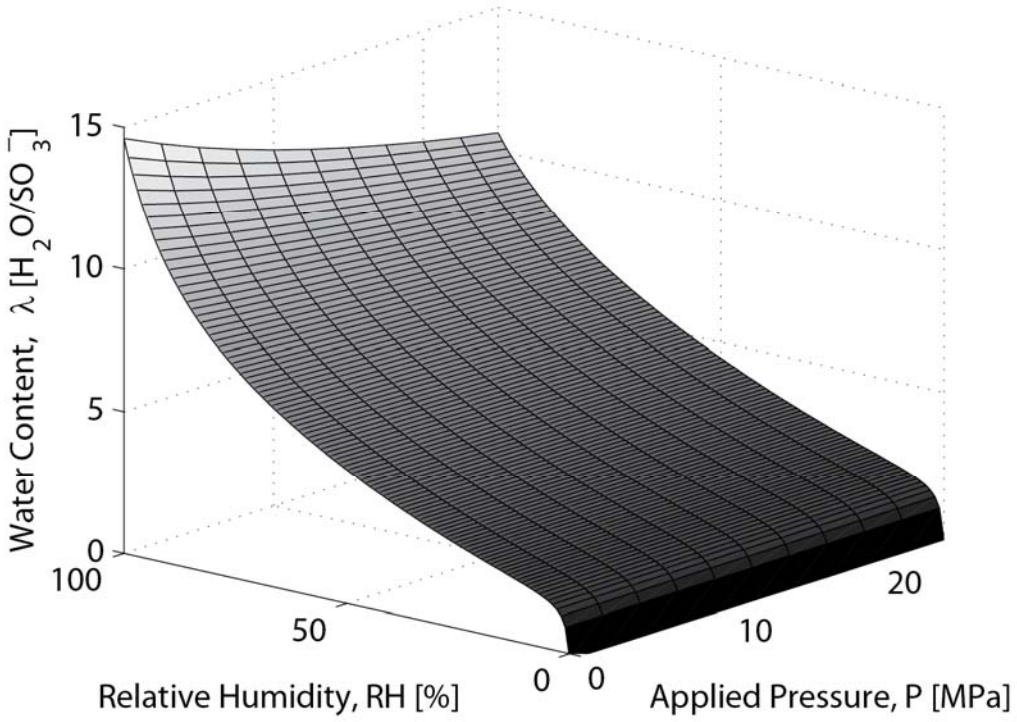

Figure 9 Predicted effect of hydrostatic pressure on the membrane sorption isotherm at 25°C (using the swelling pressure function Eq. [17] with k_c = 7.5).

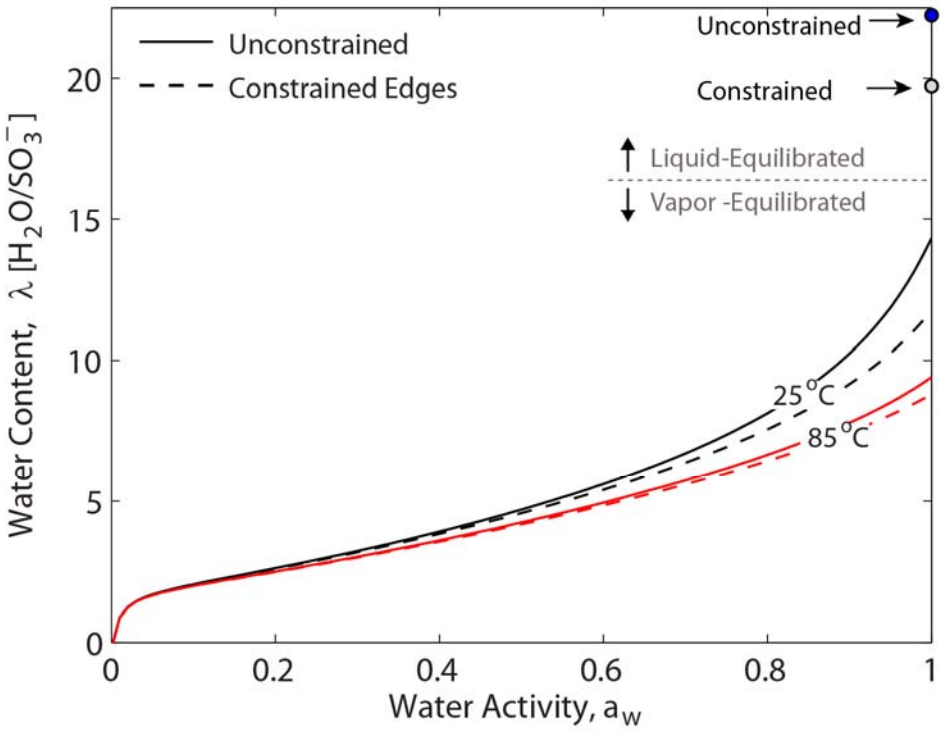

Figure 10 Model predictions for the sorption isotherms of a vapor-equilibrated membrane at 25 and 85°C and water content of a liquid-equilibrated membrane at 85°C when the membrane is unconstrained and constrained. (Constrained membrane cannot expand in the plane but is free to expand in the thickness direction.)

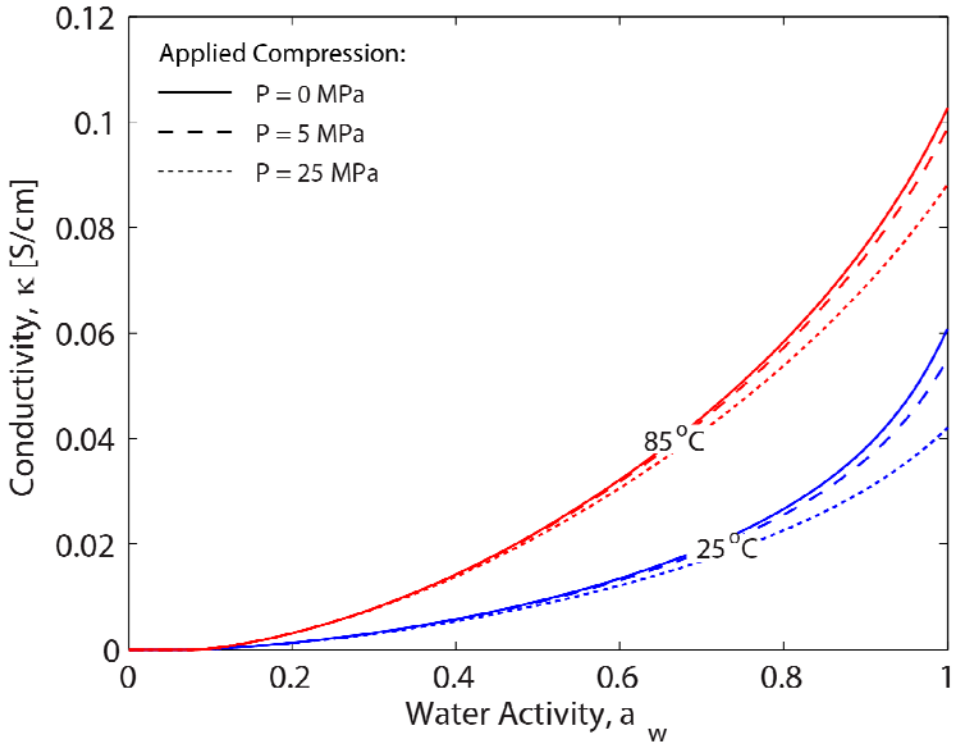

Figure 11 Model predictions for the conductivity of uncompressed and compressed membranes as a function of water activity at 25 and 85°C.